Accounting for Near-normal Glucose Sensitivity in Kir6.2[AAA] Transgenic Mice

Krasimira Tsaneva-Atanasova[1]
Laboratory of Biological Modeling, NIDDK
NIH, Bethesda, MD

Arthur Sherman[2]
Laboratory of Biological Modeling, NIDDK
NIH, Bethesda, MD

July 28, 2009

[1]Present Address: Department of Engineering Mathematics, University of Bristol, Bristol BS8 1TR, UK

[2]Corresponding author. Address: Laboratory of Biological Modeling, NIDDK, National Institutes of Health, 12 South Drive, Room 4007, Bethesda, MD 20892, U.S.A., Tel.: 301-496-4325, Fax: 301-402-0535, Email: asherman@nih.gov

Abstract

Kir6.2[AAA] transgenic mouse islets exhibit mosaicism such that approximately 70% of the β-cells have non-functional ATP-sensitive potassium ($\mathrm{K_{ATP}}$) channels, whereas the remainder have normal $\mathrm{K_{ATP}}$ function (1, 2). In spite of this drastic reduction, the glucose dose-response curve is only shifted by about 2 mM. We use a previously published mathematical model (3), in which $\mathrm{K_{ATP}}$ conductance is increased by rises in cytosolic calcium through indirect effects on metabolism, to investigate how cells could compensate for the loss of $\mathrm{K_{ATP}}$ conductance. Compensation is favored by the assumption that only a small fraction of $\mathrm{K_{ATP}}$ channels are open during oscillations, which renders it easy to up-regulate the open fraction via a modest elevation of calcium. We show further that strong gap-junctional coupling of both membrane potential and calcium is needed to overcome the stark heterogeneity of cell properties in these mosaic islets.

Key words: ATP-sensitive $\mathrm{K^+}$ channels; Mathematical model; Bifurcation theory; Coupled oscillators; Diffusion; Synchronization

1 Introduction

ATP-sensitive potassium channels are key regulators of glucose homeostasis in insulin-secreting β-cells in the pancreatic islets of Langerhans. Their conductance for K^+ is affected by changes in nucleotide levels, and these channels can thereby couple plasma membrane electrical activity to cell metabolism (4–7). When blood glucose levels are low, glycolysis in β-cells is limited by the low influx of glucose, and the intracellular ADP/ATP ratio is high. Under these conditions, $\mathrm{K_{ATP}}$ channels in the membrane of β-cells remain open, holding the membrane potential at about -70 mV. The negative membrane potential keeps voltage-dependent Ca^{2+} channels shut and the intracellular Ca^{2+} concentration low. With such limited Ca^{2+} entry, no insulin is released. When blood glucose levels are high, more glucose is taken up, glycolysis is increased, and the intracellular ADP/ATP ratio decreases. The decreased intracellular ADP/ATP ratio closes most of the $\mathrm{K_{ATP}}$ channels (8–14); more than 97% of the $\mathrm{K_{ATP}}$ channels are closed at physiological stimulatory glucose concentrations. This allows the membrane potential to become more positive, opening the voltage-gated Ca^{2+} channels and raising the intracellular Ca^{2+} concentration inside the cell. The influx of Ca^{2+} both contributes to the ensuing oscillations of electrical activity and stimulates the release of insulin from secretory vesicles (15, 16).

Thus, closing of the $\mathrm{K_{ATP}}$ channels represents a crucial step in the complex chain of events that links a rise in blood glucose concentration to insulin release (1, 16–20). Various mutations that directly or indirectly affect β-cell $\mathrm{K_{ATP}}$ channel function decouple insulin release from blood glucose concentration to in different ways and degrees. Accumulating evidence (1, 5, 16, 17, 19–21) links such mutations to a broad range of diseases from Hyperinsulinism to DEND (Development delay, Epilepsy, and Neonatal Diabetes) and type 2 diabetes. Therefore, experimental and modeling studies of the behavior of islets of Langerhans taken from animals with genetically modified $\mathrm{K_{ATP}}$ channel activity can give valuable insight into the mechanisms of regulation of these channels.

The focus of this paper is a theoretical investigation of the previously reported behavior of Kir6.2[AAA] transgenic mice, whose islets exhibit mosaicism such that about $2/3$ of the β-cells have non-functional $\mathrm{K_{ATP}}$ channels (1, 2, 21). Despite the substantial reduction in the number of functional $\mathrm{K_{ATP}}$ channels, these studies found nearly normal calcium responses and only a small shift of approximately 2-3 mM in the glucose dose-response curve. We show that a previously published model of pancreatic β-cell electrical activity (3) is able to reproduce the experimental findings, and we use bifurcation analysis to interpret the model's behavior.

In Section 2 we describe the model, modified from one of the models in (3) that

produces fast bursting (period $<$ one minute) involving oscillations in $\mathrm{K_{ATP}}$ conductance. Although similar results can be obtained with a model in which $\mathrm{K_{ATP}}$ conductance is constant, we choose this one since *a priori* it seems more challenging for a model that depends on oscillations in $\mathrm{K_{ATP}}$ conductance to compensate for the reduced $\mathrm{K_{ATP}}$ conductance.

In Section 3 we study the behavior of the model in the cases of normal (WT) islet and mutant (AAA) islets. We consider first a simplified case of perfectly coupled islets, in which membrane potential, calcium, and nucleotide concentrations are uniform and can be represented by a single cell with a reduction of $2/3$ of its functional $\mathrm{K_{ATP}}$ channels. We find that the model can compensate for this reduction by increasing the fraction of open $\mathrm{K_{ATP}}$ channels, mediated by an increase in intracellular calcium concentration. We then fit experimental data (22, 23) relating changes in external glucose concentration to the plateau fraction of bursting in order to calculate the glucose dose-response curve for the model. The results agree with the observed modest shift of approximately 2-3 mM in Kir6.2[AAA] islets (1, 2, 21). We apply bifurcation analysis of the simplified model to show geometrically how the compensation is achieved. Finally, we study a model islet consisting of 216 coupled β-cells in a cubic lattice, with $2/3$ of the cells randomly assumed to lack $\mathrm{K_{ATP}}$ channels. These simulations confirm that electrical coupling among those drastically heterogeneous β-cells can account for the nearly normal response to glucose stimulation. However, the model indicates that coupling through diffusion of calcium through gap junctions may be needed in addition to coupling via membrane potential in order to equalize $\mathrm{Ca^{2+}}$ responses in a mosaic islet. We also contrast the AAA islets with islets that are heterozygous for a different mutation (21) in Kir6.2 or in SUR1, another component of the $\mathrm{K_{ATP}}$ channel, and have a similar reduction in $\mathrm{K_{ATP}}$ conductance, but uniformly among the cells, rather than in a mosaic pattern.

2 Modeling and Methods

In the first models for β-cell bursting (24) the slow negative feedback for oscillations was provided by $\mathrm{Ca^{2+}}$-activated $\mathrm{K^+}$ channels. $\mathrm{K_{ATP}}$ current was added later as a modulating current to transduce the effects of glucose metabolism (23). There is, however, more recent experimental evidence (18, 25–28) that glucose metabolism results in oscillations in the ADP/ATP ratio, which would in turn lead to oscillations in $\mathrm{K_{ATP}}$ channel activity and hence membrane potential. $\mathrm{K_{ATP}}$ channels would then participate in the pacemaking of bursting β-cells electrical activity together with $\mathrm{Ca^{2+}}$-activated $\mathrm{K^+}$ channels.

We use a modified version of the bursting model with three slow variables

described in (3), which is based on the hypothesis that rises in Ca^{2+} increase the ADP/ATP ratio. The parameter values are given in Table 1. A few have been changed from (3), mainly an increase in $\bar{g}_{\mathrm{K_{ATP}}}$ so that it can be interpreted as the total $\mathrm{K_{ATP}}$ conductance in the cell, rather than the residual conductance at stimulatory glucose; this also entails a change in the range of values of r. The decrease in s_a was chosen to limit the shift in the glucose dose response curve. The equations for membrane potential, V, delayed rectifier activation, n, cytosolic free Ca^{2+} concentration, c, the concentration of Ca^{2+} in the endoplasmic reticulum (ER), c_{er} are as follows:

$$C_{\mathrm{m}}\frac{dV^{(\mathrm{i})}}{dt} = -(I_{\mathrm{Ca}}^{(\mathrm{i})} + I_{\mathrm{K}}^{(\mathrm{i})} + I_{\mathrm{K_{Ca}}}^{(\mathrm{i})} + I_{\mathrm{K_{ATP}}}^{(\mathrm{i})} + I_{\mathrm{c}}^{(\mathrm{i})}), \quad (1)$$

$$\frac{dn^{(\mathrm{i})}}{dt} = \frac{n_{\infty}^{(\mathrm{i})}(V^{(\mathrm{i})}) - n^{(\mathrm{i})}}{\tau_{\mathrm{n}}}, \quad (2)$$

$$\frac{dc^{(\mathrm{i})}}{dt} = f_{\mathrm{cyt}}(J_{\mathrm{mem}}^{(\mathrm{i})} + J_{\mathrm{er}}^{(\mathrm{i})} - J_{\mathrm{diff}}^{(\mathrm{i})}), \quad (3)$$

$$\frac{dc_{\mathrm{er}}^{(\mathrm{i})}}{dt} = -f_{\mathrm{er}}(V_{\mathrm{cyt}}/V_{\mathrm{er}})J_{\mathrm{er}}^{(\mathrm{i})}, \quad (4)$$

where the superscripts (i) index each variable for cell number for islet calculations. In order to carry out bifurcation analysis, we also consider a simplified case of perfectly coupled islets that can be represented by a single cell. In all cases, C_{m} is the membrane capacitance, τ_{n} is the activation time constant for the delayed rectifier channel, $n_{\infty}^{(\mathrm{i})}$ is the steady-state function for the activation variable n, $J_{\mathrm{mem}}^{(\mathrm{i})}$ and $J_{\mathrm{er}}^{(\mathrm{i})}$ are the Ca^{2+} fluxes through the plasma membrane and the ER membrane respectively. The ionic currents in Eqn. 1 are

$$I_{\mathrm{Ca}}^{(\mathrm{i})}(V^{(\mathrm{i})}) = g_{\mathrm{Ca}}m_{\infty}^{(\mathrm{i})}(V^{(\mathrm{i})})(V^{(\mathrm{i})} - V_{\mathrm{Ca}}), \quad (5)$$

$$I_{\mathrm{K}}^{(\mathrm{i})}(V^{(\mathrm{i})}, n^{(\mathrm{i})}) = g_{\mathrm{K}}n^{(\mathrm{i})}(V^{(\mathrm{i})} - V_{\mathrm{K}}), \quad (6)$$

$$I_{\mathrm{K_{Ca}}}^{(\mathrm{i})}(V^{(\mathrm{i})}, c^{(\mathrm{i})}) = g_{\mathrm{K_{Ca}}}\omega(c^{(\mathrm{i})})(V^{(\mathrm{i})} - V_{\mathrm{K}}), \quad (7)$$

$$I_{\mathrm{K_{ATP}}}^{(\mathrm{i})}(V^{(\mathrm{i})}) = g_{\mathrm{K_{ATP}}}(V^{(\mathrm{i})} - V_{\mathrm{K}}). \quad (8)$$

The steady-state activation functions are

$$m_{\infty}^{(\mathrm{i})}(V^{(\mathrm{i})}) = \left(1 + \exp\left(\frac{\nu_m - V^{(\mathrm{i})}}{s_m}\right)\right)^{-1}, \quad (9)$$

$$n_{\infty}^{(\mathrm{i})}(V^{(\mathrm{i})}) = \left(1 + \exp\left(\frac{\nu_n - V^{(\mathrm{i})}}{s_n}\right)\right)^{-1}. \quad (10)$$

The function $\omega(c^{(\mathrm{i})})$ represents the fraction of Ca^{2+}-sensitive K^+ (K_{Ca}) channels that are activated by cytosolic Ca^{2+}:

$$\omega(c^{(\mathrm{i})}) = \frac{{c^{(\mathrm{i})}}^{\mathrm{p}}}{{c^{(\mathrm{i})}}^{\mathrm{p}} + k_D^{\mathrm{p}}}, \tag{11}$$

where k_D is the dissociation constant for Ca^{2+} binding to the channel. Ca^{2+} fluxes across the plasma membrane, $J_{\mathrm{mem}}^{(\mathrm{i})}$, and the ER membrane, $J_{\mathrm{er}}^{(\mathrm{i})}$, are given by

$$J_{\mathrm{mem}}^{(\mathrm{i})}(V^{(\mathrm{i})}, c^{(\mathrm{i})}) = -(\alpha I_{\mathrm{Ca}}^{(\mathrm{i})}(V^{(\mathrm{i})}) + k_{\mathrm{PMCA}} c^{(\mathrm{i})}), \tag{12}$$

$$J_{\mathrm{er}}^{(\mathrm{i})}(c^{(\mathrm{i})}, c_{\mathrm{er}}^{(\mathrm{i})}) = p_{\mathrm{leak}}(c_{\mathrm{er}}^{(\mathrm{i})} - c^{(\mathrm{i})}) - k_{\mathrm{SERCA}} c^{(\mathrm{i})}, \tag{13}$$

where α converts current to flux, p_{leak} is the permeability of the ER membrane, and k_{PMCA} and k_{SERCA} are the plasma membrane and ER Ca^{2+} ATPase pump rates, respectively. Since c and c_{er} represent the free Ca^{2+} concentration in the cytosol and the ER, respectively, we multiply the corresponding fluxes in Eq. (3) and Eq. (4) by the fraction of free to total cytosolic Ca^{2+}, f_{cyt}, and ER Ca^{2+}, f_{er}. For the ER Ca^{2+} concentration, the flux $J_{\mathrm{er}}^{(\mathrm{i})}$ has also to be scaled by the ratio of the volumes of the cytosolic compartment, V_{cyt}, and the ER compartment, V_{er}.

In Eqn. (8), the $\mathrm{K}_{\mathrm{ATP}}$ conductance is given by

$$g_{\mathrm{K}_{\mathrm{ATP}}} = \bar{g}_{\mathrm{K}_{\mathrm{ATP}}} a^{(\mathrm{i})}, \tag{14}$$

where $\bar{g}_{\mathrm{K}_{\mathrm{ATP}}}$ is the maximum $\mathrm{K}_{\mathrm{ATP}}$ channel conductance and a is the fraction of open $\mathrm{K}_{\mathrm{ATP}}$ channels. The open fraction depends on the nucleotide concentrations and can be interpreted roughly as the ratio of ADP to ATP in the cell, which is assumed in the model to be regulated dynamically by the Ca^{2+} concentration. Thus, one more equation is added to Eqns. (1)–(4):

$$\frac{da^{(\mathrm{i})}}{dt} = \frac{a_\infty^{(\mathrm{i})}(c^{(\mathrm{i})}) - a^{(\mathrm{i})}}{\tau_{\mathrm{a}}}. \tag{15}$$

The time constant τ_{a} is large, so a slowly follows the steady-state function $a_\infty^{(\mathrm{i})}$, which has an increasing sigmoidal dependence on cytosolic Ca^{2+} concentration:

$$a_\infty^{(\mathrm{i})}(c^{(\mathrm{i})}) = \left(1 + \exp\left(\frac{r - c^{(\mathrm{i})}}{s_a}\right)\right)^{-1}. \tag{16}$$

This incorporates the effect of increasing glucose concentration through the parameter r and admits a phenomenological interpretation of the hypothesized negative feedback of Ca^{2+} on the ATP concentration as resulting from either stimulated

ATP hydrolysis or inhibited ATP production (18, 25–29). In either case, $\mathrm{K_{ATP}}$ conductance provides slow negative feedback to increases in c, which complements the rapid negative feedback provided by $g_{\mathrm{K_{Ca}}}$.

The model considered has been incorporated as a subset into a more recent model that includes in addition oscillations in glycolysis to produce slow bursting (period up to five minutes) and combined fast and slow oscillations (30). We use the sub-model because we only have data on fast oscillations in AAA islets to compare to.

The homogeneous islet model (representative single cell) is appropriate for studying the effects of $\mathrm{K_{ATP}}$ mutations on cell dynamics and bifurcation structure, but we are also interested in how much gap junctional coupling is needed to synchronize β-cells with different expression levels of functional $\mathrm{K_{ATP}}$ channels. To assess this, we incorporate both electrical and calcium coupling by adding the following gap-junctional conductance terms to the equations for V and c, respectively Eq. (1) and Eq. (3):

$$I_{\mathrm{c}}^{(\mathrm{i})}(V^{(\mathrm{i})}) = \sum_{\mathrm{j}\in\Gamma_{\mathrm{i}}} g_{\mathrm{c,V}}(V^{(\mathrm{i})} - V^{(\mathrm{j})}), \tag{17}$$

$$J_{\mathrm{diff}}^{(\mathrm{i})}(c^{(\mathrm{i})}) = \sum_{\mathrm{j}\in\Gamma_{\mathrm{i}}} g_{\mathrm{c,Ca}}(c^{(\mathrm{i})} - c^{(\mathrm{j})}). \tag{18}$$

where $g_{\mathrm{c,V}}$ and $g_{\mathrm{c,Ca}}$ are the coupling conductance and the gap-junctional permeability for Ca^{2+}, respectively, and the sum is taken over the set Γ_{i} of nearest neighbor cells to which cell (i) is coupled. In addition to the dependent variables and other expressions noted above, $\bar{g}_{\mathrm{K_{ATP}}}$ is indexed by the cell number (i) to represent mosaicism.

The model Eqns. (1)-(4), (15) for the homogeneous islet case were solved numerically using the software package XPPAUT (31). The bifurcation analysis was performed with AUTO 2000 (32). For the simulations of many coupled cells, we used a fourth-order Runge-Kutta method implemented in Fortran 95. The computer code used in the simulations can be downloaded from
http://lbm.niddk.nih.gov/sherman/.

3 Results

3.1 Compensation for reduced $\mathrm{K_{ATP}}$ conductance in AAA islets

In Fig. 1 we simulate the behavior of WT and AAA (1, 2) islets, assuming that they are sufficiently tightly coupled that each β-cell behaves more or less as the rest of the cells, and the islet can be approximated by a single representative β-cell (33).

This simplification allows us to use the system of Eqs. (1)-(4), (15) with $(\mathrm{i}) = 1$, *i. e.* in the case of a single cell, in order to simulate islet behavior.

The parameter $\bar{g}_{\mathrm{K_{ATP}}}$ represents the maximum nucleotide-sensitive K^+ conductance or, in other words, the $\mathrm{K_{ATP}}$ conductance when all $\mathrm{K_{ATP}}$ channels are open. Since in AAA islets the $\mathrm{K_{ATP}}$ channels in approximately 70% of the β-cells are non-functional whereas the remaining cells have normal $\mathrm{K_{ATP}}$ function (1, 2), we simulate the perfectly coupled AAA islet by reducing the total $\mathrm{K_{ATP}}$ conductance by $2/3$ from $\bar{g}_{\mathrm{K_{ATP}}} = 30000$ pS (WT) to $\bar{g}_{\mathrm{K_{ATP}}} = 10000$ pS (AAA). The simulations in Fig. 1 (a) indicate that the three-fold reduction of the $\mathrm{K_{ATP}}$ conductance is compensated by an increase in the fraction of open $\mathrm{K_{ATP}}$ channels. With glucose concentration, represented indirectly by the parameter r, kept fixed here at 0.2 μM, the open fraction is increased a little less than three-fold, resulting in a slightly smaller active $\mathrm{K_{ATP}}$ conductance and bursting with slightly increased plateau fraction (Fig. 1 (b)). If the value of r is reduced slightly, the open fraction and plateau fraction would be equalized, which can be interpreted as a shift in the glucose dose-response curve, as discussed in the next section. The increase in $\mathrm{K_{ATP}}$ channel open fraction is mediated by a small rise in cytosolic Ca^{2+} (Fig. 1 (c)), which is sufficient to raise the ADP/ATP ratio via the mechanism represented in Eqs. (15), (16). The increase in Ca^{2+} results as well in an increase in c_{er} (Fig. 1 (d)).

The behavior of the model when the $\mathrm{K_{ATP}}$ conductance decreases is consistent with the spare channel hypothesis (11). Since most of the $\mathrm{K_{ATP}}$ channels are closed under normal physiological stimulation (8–14) there are still plenty of spare channels that can be opened to provide $\mathrm{K_{ATP}}$ current sufficient to produce bursting electrical activity even in a situation like the AAA islets where approximately $2/3$ of the $\mathrm{K_{ATP}}$ channels are not functional (1, 2).

3.2 Glucose dose-response curve

Having shown that the model can explain the compensation for reduced $\mathrm{K_{ATP}}$ conductance, we continue by investigating whether the model can reproduce the reported modest shift in the glucose dose response of AAA islets compared to WT (1, 2, 21). In order to produce dose-response curves with the model we need to map glucose concentration to values of r. We do this by mapping burst plateau fraction to r, as done in (23), shown in Fig. 2(a), and then mapping glucose concentration to burst plateau fraction (22), shown in Fig. 2(b). The mapping from glucose to r, which is assumed to be the same for both WT and AAA, is shown in Fig. 2(c). Although secretion depends on a metabolic coupling factor or factors and can increase in constant Ca^{2+} (34–36), plateau fraction is an appropriate surrogate for secretion averaged over one hour in static incubation. In agreement with

experimental results (see (1, Fig. 4A), (21, Fig. 5), and (2, Fig. 1E)), we find only a modest shift of 2–3 mM glucose in the dose-response curve for the AAA islet compared to the WT islet.

Whereas Fig. 1 shows that at a given value of r, there is only a small change in plateau fraction as a result of the reduction in $\bar{g}_{\mathrm{K_{ATP}}}$, Fig. 2 shows that compensation for the reduction in $\bar{g}_{\mathrm{K_{ATP}}}$ requires only a small change in r to achieve the same plateau fraction. This small change represents the extent to which the rise in Ca^{2+} falls short of full compensation and which must be made up by a reduction in glucose concentration. In the next section we examine the model from a geometrical viewpoint to see how these features come about.

3.3 Bifurcation Analysis of the Single-Cell Model

In order to gain a deeper understanding of which properties of the model give it the ability to adapt to a significantly reduced number of functional $\mathrm{K_{ATP}}$ channels with little change in the calcium dynamics and the glucose dose response curve, we carry out a fast-slow bifurcation analysis of Eqs. (1)-(4) and (15).

Since this system has more than one slow variable, there are several possible ways to divide it into fast and slow sub-systems. We treat the fraction of open $\mathrm{K_{ATP}}$ channels, a, and the ER calcium concentration, c_{er}, as bifurcation parameters, and, in contrast to the approach in (3), we treat the cytosolic Ca^{2+} concentration, c, as a fast variable; the fast sub-system then consists of Eqns. (1)-(3). Fig. 3 (a) shows the bifurcation diagram with the fraction of open $\mathrm{K_{ATP}}$ channels, a, as the main bifurcation parameter and c as the output variable for both wild-type ($\bar{g}_{\mathrm{K_{ATP}}} = 30000$ pS) and mutant ($\bar{g}_{\mathrm{K_{ATP}}} = 10000$ pS) islets. The slow variation of c_{er} sweeps the z-shaped slow manifold to the right as c_{er} increases during the active phase and back to the left as c_{er} decreases during the silent phase. To indicate this, the z-curves are plotted for three different values of c_{er}, corresponding to the minimum, average and maximum attained during the oscillations. To keep the figure simple, the periodic branches are shown only for the average values of c_{er}. Finally, the Ca^{2+} vs a trajectories are superimposed and are seen to follow the paths predicted by the locations of the left knee and the terminations of the periodic branches.

The most prominent feature of the diagram is that decreasing $\bar{g}_{\mathrm{K_{ATP}}}$ shifts the steady-state curves to the right and slighly upward, corresponding to the three-fold increase in the fraction of open $\mathrm{K_{ATP}}$ channels and the small increase in the level of Ca^{2+} that produces it. The behavior of the system is also determined by the nullcline for a, particularly its intersection with the z-curve, which determines the unstable steady state of the full system, Eqns. (1)-(4), (15). Bursting oscillations are obtained approximately when the nullcline crosses the z-curve along the middle branch of saddle points, the portion that slopes up and to the right. When the

nullcline intersects the bottom branch, the solution is a steady state, and, roughly, when it intersects the periodic branch, the solution takes the form of continuous spiking. The a nullcline translates upward as the glucose-sensing parameter r increases, and the steeply rising portion of the plateau fraction vs. r curve in Fig. 2 (a) thus corresponds to the interval of r values for which the intersection of the a nullcline and the z-curve traverses the region between the left knee and the periodic branch termination. The plateau fraction increases monotonically as the intersection moves up to the right because the flow becomes slower in the active phase and faster in the silent phase.

Examination of the bifurcation diagram with this in mind suggests that the modest shift in the glucose dose response curve shown in Fig. 2 (b) is a consequence of the nearly horizontal slope of the a nullcline. That is, for fixed r, the system with reduced $\bar{g}_{\mathrm{K_{ATP}}}$ has an intersection that lies closer to the periodic branch, and hence exhibits larger plateau fraction, but only a small decrease in r is required to move the intersection back down to a level that corresponds to the same plateau fraction. Fig. 3 (b) shows that shifting r from 0.2 to 0.1885 μM shifts the a nullcline down so that the it intersects the z-curve for $\bar{g}_{\mathrm{K_{ATP}}} = 10000$ pS at the same Ca^{2+} value as the unshifted nullcline intersects the z-curve for $\bar{g}_{\mathrm{K_{ATP}}} = 30000$ pS. This results (not shown) in about the same average level of active $g_{\mathrm{K_{ATP}}}$ conductance ($\approx$ 245 pS) and about the same plateau fraction (≈ 0.25). The small shift in r required to equalize the plateau fraction reflects the small shift in the glucose dose-response curve produced by the model.

Fig. 3 (b) suggests that at $r = 0.2$ μM, cytosolic Ca^{2+} oscillations will still be obtained even when the maximum $\mathrm{K_{ATP}}$ conductance is reduced by 98% ($\bar{g}_{\mathrm{K_{ATP}}} = 600$ pS). In this case, however, the levels of cytosolic Ca^{2+} and the plateau fraction would be elevated to a much greater extent. At $\bar{g}_{\mathrm{K_{ATP}}}$= 500 pS, bursting is no longer possible for this value of r, because the a nullcline intersects too deeply into the periodic branch, and if $\bar{g}_{\mathrm{K_{ATP}}}$ is reduced further to 200 pS, only continuous spiking can be obtained, regardless of the value of r. Note, however, that even at $\bar{g}_{\mathrm{K_{ATP}}}$ = 600 pS, bursting may be prevented by a further, biophysical restriction. This would require a to have an average value of about 0.38, whereas the experiments in (8, 13, 25, 37) indicate that even in 0 glucose, only about 20% of the total $g_{\mathrm{K_{ATP}}}$ conductance in the cell would be opened. (Washing out all the cell's ATP can open up the rest.) If this bound is to be respected, then the model predicts bursting only for $\bar{g}_{\mathrm{K_{ATP}}}$ greater than about 1200 pS.

If the a nullcline is made less flat by increasing s_a from 0.01 to 0.1, similar results are obtained (Fig. 4). Oscillations with little change in Ca^{2+} levels and plateau fraction can again be obtained when $g_{\mathrm{K_{ATP}}}$ is reduced by $2/3$ (not shown), but the shift in the dose response curve is approximately doubled to about 4 mM.

In order to investigate further the robustness of the small dose response shift,

we also considered the possibility that the wild-type value of $\bar{g}_{\mathrm{K_{ATP}}}$ is four times smaller (7500 pS) than in Fig. 1, with glucose remapped to r such that the mean $\mathrm{K_{ATP}}$ open fraction is four-fold higher than in Fig. 1 for the same glucose level. The shift in the dose response curve (not shown) is only slightly larger than in Fig. 2; it shifts about 2 – 3 mM in glucose for the AAA case, which now corresponds to $\bar{g}_{\mathrm{K_{ATP}}} = 2500$ pS.

3.4 Coupled Mosaic Islets

The preceding sections have shown that a mosaic islet in which 1/3 of the cells have functional $\mathrm{K_{ATP}}$ channels can exhibit nearly normal $\mathrm{Ca^{2+}}$ oscillations provided it is very tightly coupled, such that it behaves like a single cell with 1/3 the normal conductance. It remains to show that plausible coupling strength can achieve sufficiently tight coupling. In order to investigate this, we simulate AAA islets with 216 coupled β-cell that are arranged in a 6 x 6 x 6 cube. Each cell is coupled to its nearest neighbor and has dynamics governed by Eqns. (1)-(4) and Eqn. (15). In this cubic islet the interior cells have 6 neighbors, while the peripheral cells have 3, 4 or 5 neighbors depending on their location on the islet surface. In order to achieve the mosaic expression of β-cells with functional $\mathrm{K_{ATP}}$ channels as reported in the transgenic Kir6.2[AAA] islet (1, 2, 21) we assume that $2/3$ (144) of the cells in the islet, which are randomly (uniformly) distributed, are lacking functional $\mathrm{K_{ATP}}$ channels (have $\bar{g}_{\mathrm{K_{ATP}}} = 0$ pS). The rest of the β-cells (72) are considered to be WT (have $\bar{g}_{\mathrm{K_{ATP}}} = 30000$ pS). The cells are assumed to be coupled both electrically (38–41) and through diffusion of $\mathrm{Ca^{2+}}$ via gap-junctions (42–44).

In Fig. 5 we present model simulations of such an islet where the traces are taken from a WT β-cell and a β-cell in which there are no functional $\mathrm{K_{ATP}}$ channels. Two different coupling strengths are represented in Fig. 5. The coupling strength for membrane potential in Fig. 5(b) is comparable to the experimentally measured values (45, 46), whereas that in panels (a) is increased more than four-fold. The permeability of the gap junctions for $\mathrm{Ca^{2+}}$ is not known, and has been chosen sufficiently large to synchronize as described below.

Consistent with the experiments in (2), Fig. 5(b) demonstrates that strong electrical coupling in the physiological range is sufficient to synchronize the responses in the mosaic islet. Furthermore, the top panel of Fig. 5(b) shows that the model can reproduce the experimental data showing that $\mathrm{Ca^{2+}}$ levels are equalized between mutant and wild-type cells within the islet (see Fig. 1C in (2)). This result is not obtained in the absence of diffusion of $\mathrm{Ca^{2+}}$ through the gap junctions, even with exaggerated coupling through membrane potential (not shown). The bottom panels in Fig. 5 show that coupling through $\mathrm{Ca^{2+}}$ is also able to synchronize the nucleotide ratio a and that the stronger value of diffusion of calcium through gap-

junctions is able to equalize the nucleotide ratio between the WT and mutant cells in the islet; this is a consequence of the feedback of Ca^{2+} onto ATP production (Eq. (15)), which is assumed to operate whether or not $\mathrm{K}_{\mathrm{ATP}}$ channels are present. In both Fig. 5(a) and (b), the open fraction of the WT cells agrees with the values found in the perfectly coupled islet (Fig. 1 (d)).

The most striking finding of our analysis is that although coupling strengths in the physiological range for normal islets (45, 46) are sufficient to synchronize the responses in an AAA islet (Fig. 5 (b)), they are not sufficient to produce normal bursts in the membrane potential (Fig. 5 (b) middle panel). In the simulations, the fast spikes within a burst of the membrane potential disappear by oscillator death because of the extreme heterogeneity of the mosaic islets (47). However, if the electrical and Ca^{2+} coupling are increased further (Fig. 5 (a)), the spikes in the membrane potential during the active phases of the bursts are restored even when the cells in the mutant islet are so different. In contrast, if $g_{\mathrm{K}_{\mathrm{ATP}}}$ is reduced uniformly by 2/3 in all the cells, synchrony, equalized Ca^{2+} and normal spike amplitude can be achieved with coupling only on membrane potential equal to the weaker value in Fig. 5 (not shown). This case is also of physiological interest as it corresponds to islets from mice that are heterozygous for the Kir6.2 or SUR1 genes (21).

4 Discussion

In this study we have sought to account for the nearly normal glucose sensitivity observed experimentally (1, 2, 21) in transgenic Kir6.2[AAA] islets that are characterized by mosaic structure in which approximately 70% of their β-cells lack functional $\mathrm{K}_{\mathrm{ATP}}$ channels. We adapted a previously published mathematical model (3) of β-cell electrical activity that incorporates oscillations in the fraction of open $\mathrm{K}_{\mathrm{ATP}}$ channels, which participate in the pacemaking of β-cells electrical activity together with Ca^{2+}-sensitive K^{+} channels. The oscillations in $\mathrm{K}_{\mathrm{ATP}}$ conductance reflect oscillations in the nucleotide ratio ADP/ATP that are driven by the rise and fall of cytosolic Ca^{2+}. The model is agnostic as to whether this effect is caused by increased ATP consumption (48–50) or decreased ATP production (51) or both, so our results do not depend on the answer to this question. Under this generic assumption, a three-fold reduction in $\mathrm{K}_{\mathrm{ATP}}$ conductance in AAA islets leads to a nearly three-fold increase in the fraction of open $\mathrm{K}_{\mathrm{ATP}}$ channels, which restores nearly normal oscillations (Fig. 1) as observed experimentally. This result is achieved in the model because elevated Ca^{2+} persists until the total conductance of open $\mathrm{K}_{\mathrm{ATP}}$ channels rises to the range (≈ 250 pS) needed to turn the activity off. This range is in agreement with that reported in wild-type (WT) islets

(12, 18, 52, 53).

In order to achieve an exact three-fold rise in active $\mathrm{K_{ATP}}$ conductance, glucose must be lowered in the AAA case compared to WT, that is, the glucose dose response curve shifts to the left. In order to estimate the size of the shift, we mapped the $g_{\mathrm{K_{ATP}}}$ open fraction obtained in the model as a function of the glucose-sensing parameter, r in Eq. (15). We found (Fig. 2) that the shift was about 2 mM. We then showed geometrically that this small shift was possible because of the assumed relatively steep increase in steady-state $g_{\mathrm{K_{ATP}}}$ open fraction with $\mathrm{Ca^{2+}}$ (Fig. 3). The result is not excessively sensitive to the slope of this increase, as a ten-fold reduction in the slope results in only a two-fold increase in the shift of the glucose dose response curve (Fig. 4). We also found that the modest shift in the dose response curve is not very sensitive to the assumed level of $\bar{g}_{\mathrm{K_{ATP}}}$ (not shown).

The model predicts that islets can compensate for much larger reductions in $\bar{g}_{\mathrm{K_{ATP}}}$. The most fundamental limitation is that the $\mathrm{K_{ATP}}$ open fraction cannot exceed 1; this would predict a minimum $\bar{g}_{\mathrm{K_{ATP}}}$ value at which oscillations could ever be obtained of only 100 pS, given the other parameters of the model's fast subsystem. However, long before this limit was reached, bursting would be prevented because the a nullcline would intersect the branch of periodic solutions (Fig. 3); this is predicted to occur at about $\bar{g}_{\mathrm{K_{ATP}}}$ = 500 pS. Moreover, there is experimental evidence (8, 13, 25, 37) that the fraction of open $\mathrm{K_{ATP}}$ channels in 0 glucose is ≈ 0.2. This bound would limit the residual $\mathrm{K_{ATP}}$ conductance for a mutant to about 1200 pS. Even so, that represents impressive tolerance to a decrease of 96% from 30,000 pS, or 84% from 7,500 pS.

We note that $\mathrm{Ca^{2+}}$ oscillations have been observed in islets from mice in which all $\mathrm{K_{ATP}}$ channels are lost (54, 55). The mechanism described in this paper cannot account for such behavior, and instead the existence of an alternative metabolically sensitive $\mathrm{K^{+}}$ channel has been suggested to compensate partially for the loss of $\mathrm{K_{ATP}}$ channels (54). It is possible that the compensation in AAA mutants is also due to an alternative channel. No such channel has yet been identified, however, and our model shows that it may not be required to account for the partial loss of $\mathrm{K_{ATP}}$.

A model with constant fraction of open $\mathrm{K_{ATP}}$ channels would also be able to compensate for reduction in total $\mathrm{K_{ATP}}$ conductance. In this case β-cell electrical activity would be driven by other currents, such as $\mathrm{K_{Ca}}$ current, and the role of $\mathrm{K_{ATP}}$ current would be only to trigger the bursts in the membrane potential rather than contribute to pacemaking. In this case, there would be no increase in the fraction of open $\mathrm{K_{ATP}}$ channels as a result of $\mathrm{Ca^{2+}}$ feedback and all of the burden of compensation would be borne by a reduction in glucose to increase the ratio of ADP to ATP. Thus, other things being equal, one might expect that the shift in the dose response curve when $\bar{g}_{\mathrm{K_{ATP}}}$ is reduced would be larger than in a model

with oscillating $g_{\mathrm{K_{ATP}}}$. However, the present model is very sensitive to the open fraction of $\mathrm{K_{ATP}}$ channels when that fraction is fixed independent of $\mathrm{Ca^{2+}}$, and we have not found any other satisfactory model with which to test this conjecture quantitatively. We can nonetheless conclude from the findings presented here that the ability of islets to compensate for substantial reductions in $\mathrm{K_{ATP}}$ conductance is not per se a reason to prefer models with non-oscillating $\mathrm{K_{ATP}}$ to models with oscillating $\mathrm{K_{ATP}}$.

We also examined whether gap-junctional coupling of plausible strength can produce the synchronized response in mosaic islets assumed in the above calculations. We simulated islets in which 2/3 of the cells had no $\mathrm{K_{ATP}}$ channels while 1/3 had the normal complement. Although in our simulations we used only 216 cells (arranged in a 6 x 6 x 6 cube) we have obtained qualitatively similar results (not shown) using 1728 cells (arranged in a 12 x 12 x 12 cube). As has been previously shown (56), the gap-junctional conductance required to synchronize an islet scales like the diameter of the islet. Thus, increasing the islet size from 6 x 6 x 6 to 12 x 12 x 12 would increase the conductance needed to synchronize its activity by a factor of approximately two. The simulations (Fig. 5) showed that synchrony and equalized $\mathrm{Ca^{2+}}$ between WT and mutant cells within the islet are possible only if coupling via diffusion of $\mathrm{Ca^{2+}}$ is assumed in addition to the standard coupling via membrane potential. This confirmed the suggestion that gap junctional coupling could account for the nearly normal glucose sensitivity observed experimentally in AAA islets (2). However, in order to obtain voltage bursts with spikes, rather than plateaus, the coupling for membrane potential had to be at least four-fold greater than that measured physiologically. At this time, membrane potential oscillations in AAA islets have not been studied, so we do not know if the coupling strength is up-regulated or if in fact the spikes in the burst are eliminated. On the other hand, it is possible to obtain synchronized voltage bursts without spikes in the active phase as in Fig. 5(b) if the coupling conductance is reduced to 0.2 nS because it is much easier to synchronize the slow waves than the spikes. In islets in which coupling is reduced uniformly in every cell, as in Kir6.2 +/- or SUR1 +/- mice (21) or islets with partial but uniform pharmacological blockade of $\mathrm{K_{ATP}}$ channels, the model indicates that synchrony is not a problem.

We have focused on transgenic Kir6.2[AAA] (1, 2, 21) islets and showed that reducing $\bar{g}_{\mathrm{K_{ATP}}}$results in a left shift of the glucode dose-response curve, which is partly compensated by the rise in $\mathrm{Ca^{2+}}$. Diabetes has been associated in genome scans with reduced $\mathrm{K_{ATP}}$ channel affinity for ATP. In such a case, one can expect a right shift in the glucose dose-response curve, as has been observed in transgenic mice (57). The extent of the shift as a function of the reduction in ATP sensitivity and whether the shift may be partly compensated by a fall in $\mathrm{Ca^{2+}}$ are interesting questions for future modeling studies.

5 Conclusions

The results of the study can be summarized in the following predictions about the fraction of open $\mathrm{K_{ATP}}$ channels in β-cells from WT and AAA islets, and about the effect of electrical gap-junctional coupling and calcium diffusion through gap-junctions on the collective behavior of coupled heterogeneous β-cells. We propose independent of the details of the model for electrical activity:

- *Prediction 1*: The fraction of open K^+ channels in transgenic Kir6.2[AAA] islets (1, 2, 21) is approximately 3-fold larger than in wild type islets at equivalent activity (Fig. 1 (a)).
- *Prediction 2*: Calcium diffusion through gap-junctions among the β-cells is needed to equalize $[\mathrm{Ca}^{2+}]_\mathrm{i}$ levels in the transgenic Kir6.2[AAA] islets (1, 2, 21) due to widely discrepant K^+ conductances (Fig. 5 (b)).
- *Prediction 3*: In Kir6.2[AAA] islets, either coupling is stronger than in wild-type islets (Fig. 5 (a)) or spiking is lost (Fig. 5 (b)). Kir6.2 +/- islets would not require such strong coupling because of lesser heterogeneity.

Acknowledgments. AS was supported by the intramural research program of the National Institutes of Health, NIDDK (USA). We thank Colin Nichols for discussions that were helpful in formulating the models and interpreting the data.

References

1. Koster, J. C., M. S. Remedi, T. P. Flagg, J. D. Johnson, K. P. Markova, B. A. Marshall, and C. G. Nichols, 2002. Hyperinsulinism induced by targeted suppression of β-cell $\mathrm{K_{ATP}}$ channels. *Proc Natl Acad Sci U S A* 99:16992–7.

2. Rocheleau, J. V., M. S. Remedi, B. Granada, W. S. Head, J. C. Koster, C. G. Nichols, and D. W. Piston, 2006. Critical role of gap junction coupled $\mathrm{K_{ATP}}$ channel activity for regulated insulin secretion. *PLoS Biol* 4:e26.

3. Bertram, R., and A. Sherman, 2004. A calcium-based phantom bursting model for pancreatic islets. *Bull Math Biol* 66:1313–44.

4. Ashcroft, F. M., M. Kakei, R. P. Kelly, and R. Sutton, 1987. ATP -sensitive $\mathrm{K^+}$ channels in human isolated pancreatic B-cells. *FEBS Lett* 215:9–12.

5. Ashcroft, F., 2007. The Walter B. Cannon Physiology in Perspective Lecture, 2007. ATP -sensitive $\mathrm{K^+}$ channels and disease: from molecule to malady. *Am J Physiol Endocrinol Metab* 293:E880–9.

6. Babenko, A. P., L. Aguilar-Bryan, and J. Bryan, 1998. A view of SUR/$\mathrm{K_{IR}}$6.X, $\mathrm{K_{ATP}}$ channels. *Annu Rev Physiol* 60:667–87.

7. Cook, D. L., and C. N. Hales, 1984. Intracellular ATP directly blocks $\mathrm{K^+}$ channels in pancreatic B-cells. *Nature* 311:271–3.

8. Ashcroft, F. M., S. J. Ashcroft, and D. E. Harrison, 1988. Properties of single potassium channels modulated by glucose in rat pancreatic β-cells. *J Physiol* 400:501–27.

9. Ashcroft, F. M., D. E. Harrison, and S. J. Ashcroft, 1984. Glucose induces closure of single potassium channels in isolated rat pancreatic β-cells. *Nature* 312:446–8.

10. Cook, D. L., and M. Ikeuchi, 1989. Tolbutamide as mimic of glucose on β-cell electrical activity. ATP -sensitive $\mathrm{K^+}$ channels as common pathway for both stimuli. *Diabetes* 38:416–21.

11. Cook, D. L., L. S. Satin, M. L. Ashford, and C. N. Hales, 1988. ATP -sensitive $\mathrm{K^+}$ channels in pancreatic β-cells. Spare-channel hypothesis. *Diabetes* 37:495–8.

12. Rorsman, P., and G. Trube, 1985. Glucose dependent $\mathrm{K^+}$ -channels in pancreatic β-cells are regulated by intracellular ATP . *Pflugers Arch* 405:305–9.

13. Tarasov, A., C. Girard, and F. Ashcroft, 2006. ATP sensitivity of the ATP - sensitive K^+ channel in intact and permeabilized pancreatic β-cells. *Diabetes* 55:2446–54.

14. Valdeolmillos, M., A. Nadal, D. Contreras, and B. Soria, 1992. The relationship between glucose-induced K_{ATP} channel closure and the rise in $[Ca^{2+}]_i$ in single mouse pancreatic β-cells. *J Physiol* 455:173–86.

15. Arkhammar, P., T. Nilsson, P. Rorsman, and P. O. Berggren, 1987. Inhibition of ATP -regulated K^+ channels precedes depolarization-induced increase in cytoplasmic free Ca^{2+} concentration in pancreatic β-cells. *J Biol Chem* 262:5448–54.

16. Nichols, C. G., and J. C. Koster, 2002. Diabetes and insulin secretion: whither K_{ATP} ? *Am J Physiol Endocrinol Metab* 283:E403–12.

17. Ashcroft, F. M., 2005. ATP -sensitive potassium channelopathies: focus on insulin secretion. *J Clin Invest* 115:2047–58.

18. Larsson, O., H. Kindmark, R. Brandstrom, B. Fredholm, and P. O. Berggren, 1996. Oscillations in K_{ATP} channel activity promote oscillations in cytoplasmic free Ca^{2+} concentration in the pancreatic β-cell. *Proc Natl Acad Sci U S A* 93:5161–5.

19. Koster, J. C., M. A. Permutt, and C. G. Nichols, 2005. Diabetes and insulin secretion: the ATP -sensitive K^+ channel (K_{ATP}) connection. *Diabetes* 54:3065–72.

20. Nichols, C. G., 2006. K_{ATP} channels as molecular sensors of cellular metabolism. *Nature* 440:470–6.

21. Remedi, M., J. Rocheleau, A. Tong, B. Patton, M. McDaniel, D. Piston, J. Koster, and C. Nichols, 2006. Hyperinsulinism in mice with heterozygous loss of K_{ATP} channels. *Diabetologia* 49:2368–78.

22. Meissner, H. P., and H. Schmelz, 1974. Membrane potential of β-cells in pancreatic islets. *Pflügers Arch.* 351:195–206.

23. Himmel, D., and T. R. Chay, 1987. Theoretical studies on the electrical activity of pancreatic β-cells as a function of glucose. *Biophys J* 51:89–107.

24. Chay, T. R., and J. Keizer, 1983. Minimal model for membrane oscillations in the pancreatic β-cell. *Biophys J* 42:181–190.

25. Misler, S., L. C. Falke, K. Gillis, and M. L. McDaniel, 1986. A metabolite-regulated potassium channel in rat pancreatic β-cells. *Proc Natl Acad Sci U S A* 83:7119–23.

26. Rolland, J. F., J. C. Henquin, and P. Gilon, 2002. Feedback control of the ATP -sensitive K^+ current by cytosolic Ca^{2+} contributes to oscillations of the membrane potential in pancreatic β-cells. *Diabetes* 51:376–84.

27. Kanno, T., P. Rorsman, and S. O. Gopel, 2002. Glucose-dependent regulation of rhythmic action potential firing in pancreatic β-cells by $\mathrm{K}_{\mathrm{ATP}}$ -channel modulation. *J Physiol* 545:501–7.

28. MacDonald, P. E., and P. Rorsman, 2006. Oscillations, intercellular coupling, and insulin secretion in pancreatic β-cells. *PLoS Biol* 4:e49.

29. Duchen, M. R., P. A. Smith, and F. M. Ashcroft, 1993. Substrate-dependent changes in mitochondrial function, intracellular free calcium concentration and membrane channels in pancreatic β-cells. *Biochem J* 294 (Pt 1):35–42.

30. Bertram, R., L. Satin, M. Zhang, P. Smolen, and A. Sherman, 2004. Calcium and glycolysis mediate multiple bursting modes in pancreatic islets. *Biophys J* 87:3074–3087.

31. Ermentrout, B., 2002. Simulating, Analyzing and Animating Dynamical Systems: A Guide to XPPAUT for Researchers and Students. SIAM.

32. Doedel, E., R. Paffenroth, A. Champneys, T. Fairgrieve, Y. Kuznetsov, B. Sandstede, and X. Wang, 2001. AUTO2000: Continuation and bifurcation software for ordinary differential equations (with HomCont). Technical report, Caltech.

33. Sherman, A., J. Rinzel, and J. Keizer, 1988. Emergence of organized bursting in clusters of pancreatic β-cells by channel sharing. *Biophys J* 54:411–25.

34. Grodsky, G., 1972. A threshold distribution hypothesis for packet storage of insulin and its mathematical modeling. *J Clin Invest* 51:2047–2059.

35. Henquin, J.-C., 2000. Triggering and amplifying pathways of regulation of insulin secretion by glucose. *Diabetes* 49:1751–1760.

36. Chen, Y. D., S. Wang, and A. Sherman, 2008. Identifying the targets of the amplifying pathway for insulin secretion in pancreatic β-cells by kinetic modeling of granule exocytosis. *Biophys J* 95:2226–2241.

37. Enkvetchakul, D., G. Loussouarn, E. Makhina, S. L. Shyng, and C. G. Nichols, 2000. The kinetic and physical basis of $\mathrm{K_{ATP}}$ channel gating: toward a unified molecular understanding. *Biophys J* 78:2334–48.

38. Valdeolmillos, M., A. Gomis, and J. V. Sanchez-Andres, 1996. In vivo synchronous membrane potential oscillations in mouse pancreatic β-cells: lack of co-ordination between islets. *J Physiol* 493 (Pt 1):9–18.

39. Cao, D., G. Lin, E. Westphale, E. Beyer, and T. Steinberg, 1997. Mechanisms for the coordination of intercellular calcium signaling in insulin-secreting cells. *J Cell Sci* 110:497–504.

40. Quesada, I., E. Fuentes, E. Andreu, P. Meda, A. Nadal, and B. Soria, 2003. On-line analysis of gap junctions reveals more efficient electrical than dye coupling between islet cells. *Am J Physiol Endocrinol Metab* 284:E980–987.

41. Ravier, M. A., M. Guldenagel, A. Charollais, A. Gjinovci, D. Caille, G. Sohl, C. B. Wollheim, K. Willecke, J.-C. Henquin, and P. Meda, 2005. Loss of Connexin36 Channels Alters β-Cell Coupling, Islet Synchronization of Glucose-Induced $\mathrm{Ca^{2+}}$ and Insulin Oscillations, and Basal Insulin Release. *Diabetes* 54:1798–1807.

42. Charpantier, E., J. Cancela, and P. Meda, 2007. B-cells preferentially exchange cationic molecules via connexin 36 gap junction channels. *Diabetologia* 50:2332–2341.

43. Harris, A., 2007. Connexin channel permeability to cytoplasmic molecules. *Progress in biophysics and molecular biology* 94:120–143.

44. Serre-Beinier, V., D. Bosco, L. Zulianello, A. Charollais, D. Caille, E. Charpantier, B. Gauthier, G. Diaferia, B. Giepmans, R. Lupi, et al., 2009. Cx36 makes channels coupling human pancreatic β-cells, and correlates with insulin expression. *Human Molecular Genetics* 18:428.

45. Mears, D., N. F. Sheppard, Jr., I. Atwater, and E. Rojas, 1995. Magnitude and modulation of pancreatic β-cell gap junction electrical conductance *in situ*. *J Membrane Biol* 146:163–176.

46. Göpel, S., T. Kanno, S. Barg, J. Galvanovskis, and P. Rorsman, 1999. Voltage-gated and resting membrane currents recorded from β-cells in intact mouse pancreatic islets. *J Physiol* 521 Pt 3:717–28.

47. De Vries, G., A. Sherman, and H. R. Zhu, 1999. Diffusively Coupled Bursters: Effects of Cell Heterogeneity. *Bulletin of Mathematical Biology* 61:1017.

48. Fridlyand, L. E., N. Tamarina, and L. H. Philipson, 2003. Modeling of Ca^{2+} flux in pancreatic β-cells: role of the plasma membrane and intracellular stores. *Am J Physiol (Endocrinol Metab)* 285:E138–E154.

49. Fridlyand, L. E., L. Ma, and L. H. Philipson, 2005. Adenine nucleotide regulation in pancreatic β-cells: modeling of ATP/ADP-Ca^{2+} interactions. *Am J Physiol (Endocrinol Metab)* 289:E839–E848.

50. Diederichs, F., 2006. Mathematical simulation of membrane processes and metabolic fluxes of the pancreatic β-cell. *Bull Math Biol* 68:1779–1818.

51. Magnus, G., and J. Keizer, 1997. Minimal Model of mitochondrial Ca^{2+} handling. *Am J Physiol* 273:C717–C733.

52. Smith, P. A., F. M. Ashcroft, and P. Rorsman, 1990. Simultaneous recordings of glucose dependent electrical activity and ATP-regulated K^+ -currents in isolated mouse pancreatic β-cells. *FEBS Lett* 261:187–90.

53. Kinard, T. A., G. de Vries, A. Sherman, and L. S. Satin, 1999. Modulation of the bursting properties of single mouse pancreatic β-cells by artificial conductances. *Biophys J* 76:1423–35.

54. Szollosi, A., M. Nenquin, L. Aguilar-Bryan, J. Bryan, and J.-C. Henquin, 2007. Glucose stimulates Ca^{2+} influx and insulin secretion in 2-week-old β-cells lacking ATP-sensitive K^+ channels. *J. Biol. Chem.* 282:1747–1756.

55. Düfer, M., D. Haspel, P. Krippeit-Drews, L. Aguilar-Bryan, J. Bryan, and G. Drews, 2004. Oscillations of membrane potential and cytosolic Ca^{2+} concentration in $SUR1^{-/-}$beta cells. *Diabetologia* 47:488–498.

56. De Vries, G., and A. Sherman, 2000. Channel sharing in pancreatic β-cells revisited: enhancement of emergent bursting by noise. *Journal of Theoretical Biology* 207:513–530.

57. Girard, C. A., F. T. Wunderlich, K. Shimomura, S. Collins, S. Kaizik, P. Proks, F. Abdulkader, A. Clark, V. Ball, L. Zubcevic, L. Bentley, R. Clark, C. Church, A. Hugill, J. Galvanovskis, R. Cox, P. Rorsman, J. C. Brüning, and F. M. Ashcroft, 2009. Expression of an inactivating mutation in the gene encoding the K_{ATP} channel subunit Kir6.2 in mouse pancreatic β cells recapitulates neonatal diabetes. *J. Clin. Invest.* 119:80–90.

Table of Parameter Values

r^*	0.2 μM	s_a^*	0.01 μM	C_{m}	5 300 fF
f_{cyt}; f_{er}	0.01	τ_{a}	300 000 ms	$g_{\mathrm{K_{Ca}}}$	300 pS
$V_{\mathrm{cyt}}/V_{\mathrm{er}}$	5	p_{leak}	0.0005 ms^{-1}	ν_n	-16 mV
K_{D}	0.3 μM	α	4.5$\times 10^{-6}$ fA$^{-1}\mu$M ms^{-1}	s_n	5 mV
k_{PMCA}	0.2 ms^{-1}	k_{SERCA}	0.4 ms^{-1}	ν_m	-20 mV
V_{K}	-75 mV	τ_{n}	16 ms	s_m	12 mV
V_{Ca}	25 mV	g_{K}	3 000 pS	p	5
$\bar{g}^*_{\mathrm{K_{ATP}}}$	30 000 pS	g_{Ca}	1 200 pS		

Table 1: Parameter values for Fig. 1. * indicates values modified from (3). The main change is an increase in $\bar{g}_{\mathrm{K_{ATP}}}$ so that it can be interpreted as the total $\mathrm{K_{ATP}}$ conductance in the cell, rather than the residual conductance at stimulatory glucose; this also entails a change in the range of values of r. The decrease in s_a was chosen to limit the shift in the glucose dose response curve (compare Figs. 2 and 4). Figure legends indicate variations from the table.

Table and Figure Legends

Table 1. Parameter values of the model.

Figure 1. Model simulations of WT and AAA islets. (a) Fraction of open $\mathrm{K_{ATP}}$ channels - a; (b) membrane potential - V; (c) cytosolic $\mathrm{Ca^{2+}}$ concentration - $[\mathrm{Ca^{2+}}]_{\mathrm{i}}$; (d) ER $\mathrm{Ca^{2+}}$ concentration - $[\mathrm{Ca^{2+}}]_{\mathrm{ER}}$; r = 0.2 for both islets.

Figure 2. Glucose dose-response curves for simulated of WT and AAA islets. (a) mapping of parameter r to plateau fraction. (b) mapping of glucose to plateau fraction via r. (c) mapping of glucose to r implied by (a) and (b).

Figure 3. Fast-slow analysis of the model. (a) Bifurcation diagrams for WT and AAA islets, showing the maximum and the minimum of the periodic orbits for $[\mathrm{Ca^{2+}}]_{\mathrm{i}}$ as a function of a. Superimposed on the bifurcation diagrams are the corresponding trajectories and the a nullclines for $r = 0.2$ μM and $r = 0.1885$ μM . (b) Bifurcation diagrams for WT, AAA islets, and an islet where 95% of the β-cells have non functional $\mathrm{K_{ATP}}$ channels. The broken lines in the Z-curves denote instability.

Figure 4. Glucose dose-response curves for simulated WT and AAA islets with s_a increased from 0.01 to 0.1 μM (compare Fig. 2). (a) mapping of r to plateau fraction. (b) mapping of glucose to plateau fraction via r.

Figure 5. Simulations of a mosaic AAA islet of 216 coupled cells with 2/3 of β-cells having non-functional KATP channels, 1/3 with oscillating KATP conductance. The coupling strength used in the simulations is indicated in the top panels for (a) and (b). The red curves are for a representative mutant cell, and the blue curves are for a representative wild-type cell. In the bottom panels, the nucleotide ratio a is plotted; for the wild-type cell only this also represents the open probability of the $\mathrm{K_{ATP}}$ channels.

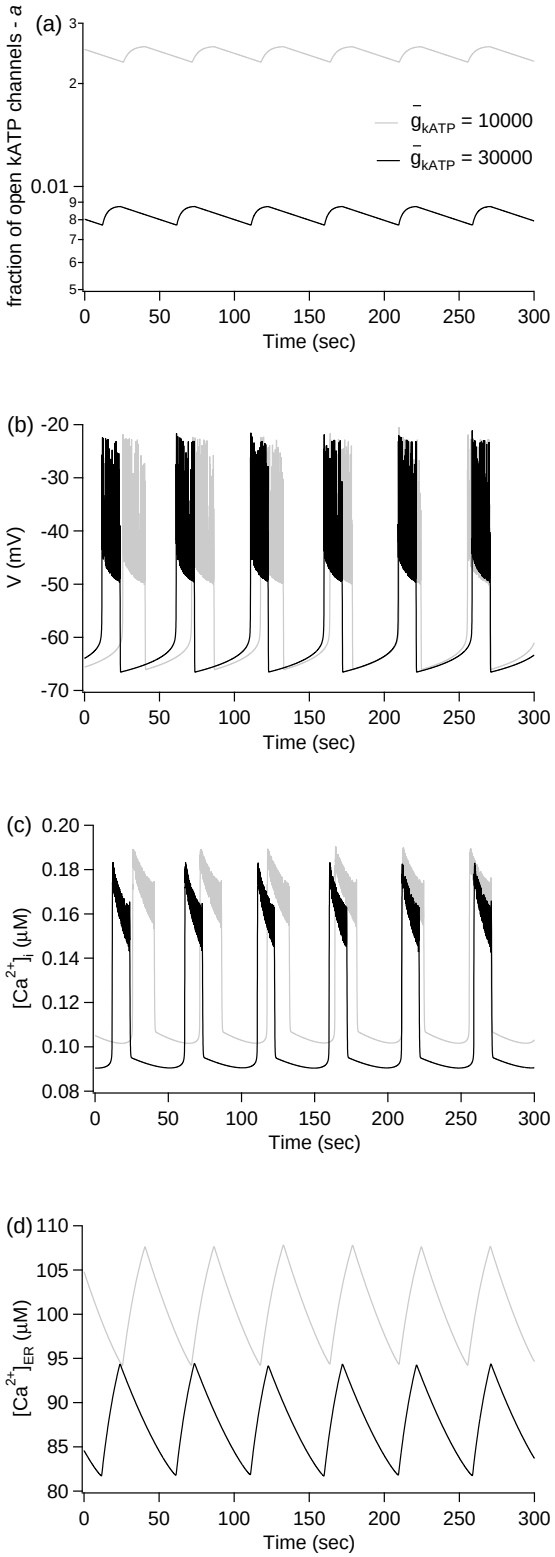
(a)
fraction of open kATP channels - a
$\bar{g}_{kATP}$ = 10000
$\bar{g}_{kATP}$ = 30000
Time (sec)
(b)
V (mV)
Time (sec)
(c)
$[Ca^{2+}]_i$ (μM)
Time (sec)
(d)
$[Ca^{2+}]_{ER}$ (μM)
Time (sec)

Figure 1:

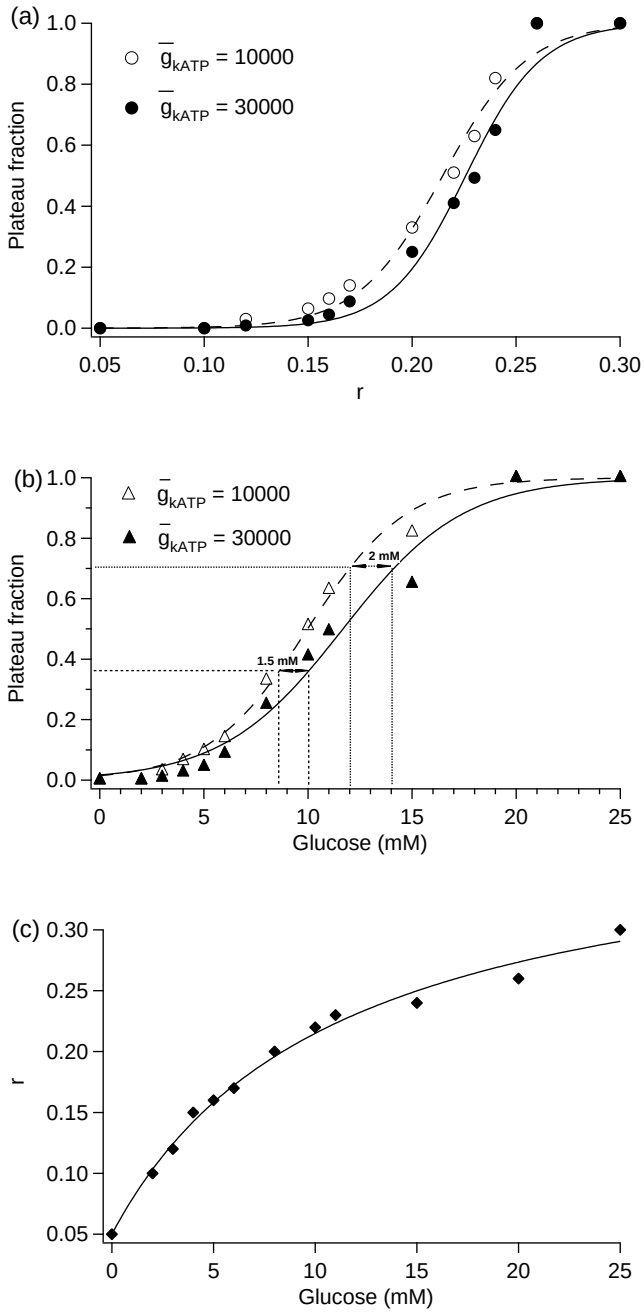
(a)
Plateau fraction
r
$\bar{g}_{kATP}$ = 10000
$\bar{g}_{kATP}$ = 30000
(b)
Plateau fraction
Glucose (mM)
$\bar{g}_{kATP}$ = 10000
$\bar{g}_{kATP}$ = 30000
1.5 mM
2 mM
(c)
r
Glucose (mM)

Figure 2:

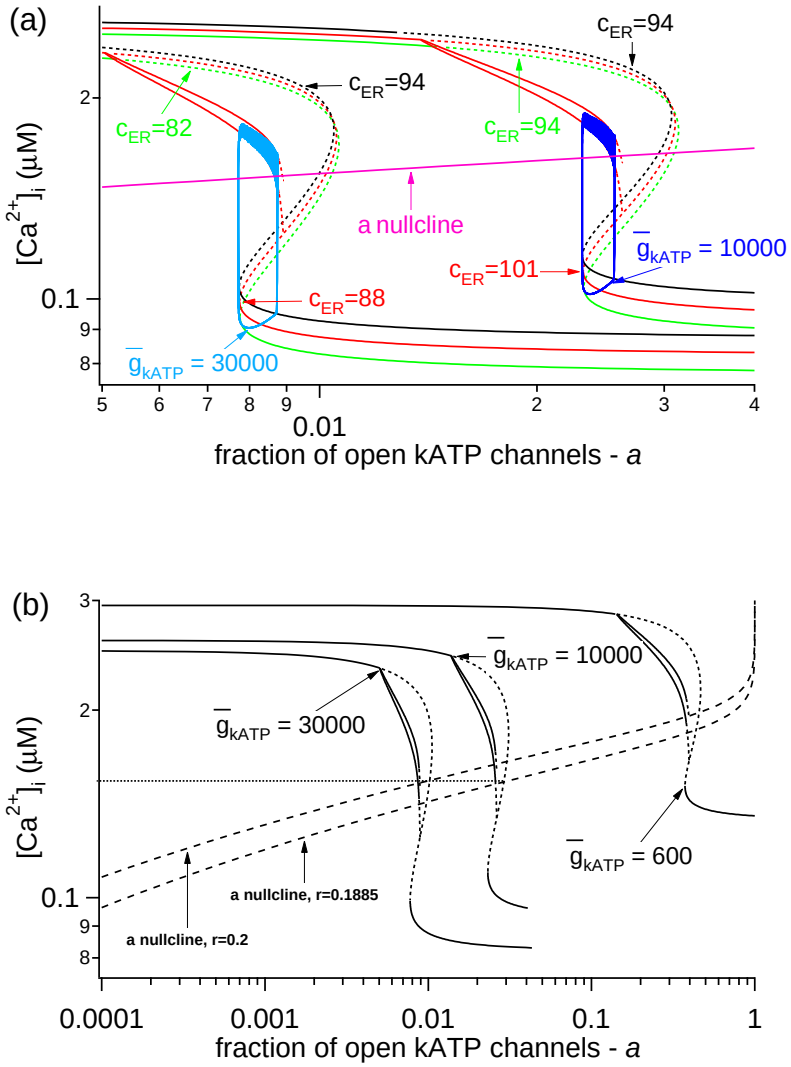
(a)
c_{ER}=94
c_{ER}=94
c_{ER}=82
c_{ER}=94
a nullcline
$\bar{g}_{kATP}$ = 10000
c_{ER}=101
c_{ER}=88
$\bar{g}_{kATP}$ = 30000
$[Ca^{2+}]_i$ (μM)
2
0.1
9
8
5
6
7
8
9
0.01
2
3
4
fraction of open kATP channels - *a*
(b)
$\bar{g}_{kATP}$ = 10000
$\bar{g}_{kATP}$ = 30000
$\bar{g}_{kATP}$ = 600
a nullcline, r=0.1885
a nullcline, r=0.2
$[Ca^{2+}]_i$ (μM)
3
2
0.1
9
8
0.0001
0.001
0.01
0.1
1
fraction of open kATP channels - *a*

Figure 3:

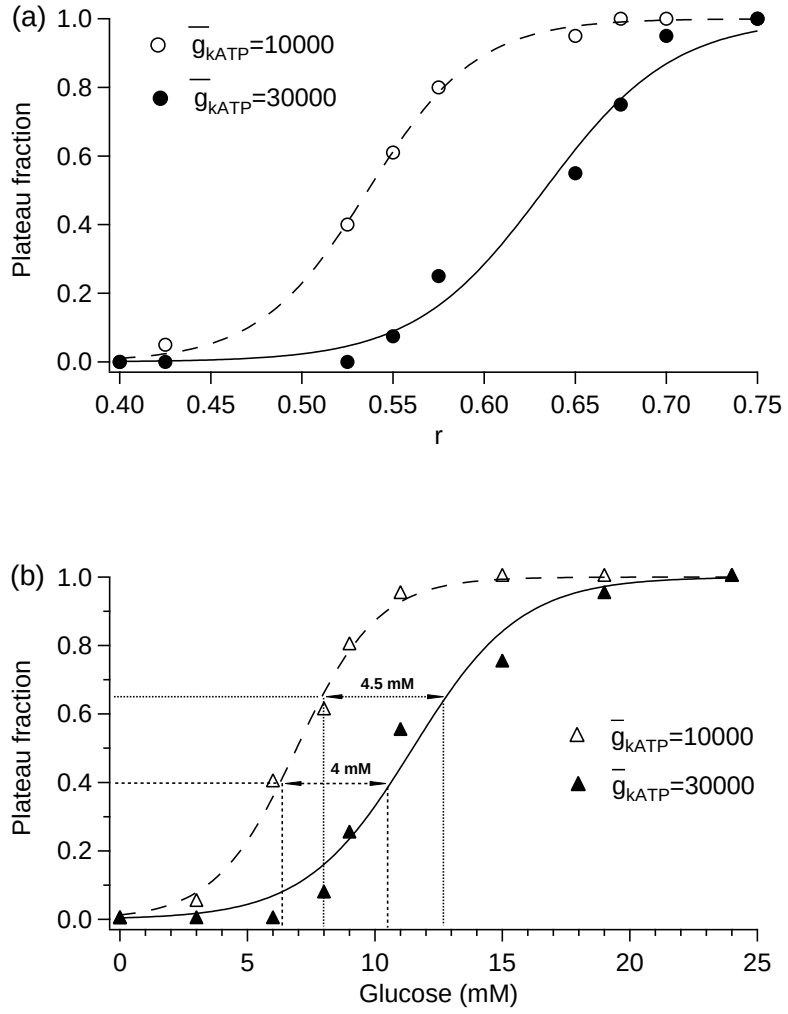
(a)
Plateau fraction
r
$\bar{g}_{kATP}$=10000
$\bar{g}_{kATP}$=30000
(b)
Plateau fraction
Glucose (mM)
4.5 mM
4 mM
$\bar{g}_{kATP}$=10000
$\bar{g}_{kATP}$=30000

Figure 4:

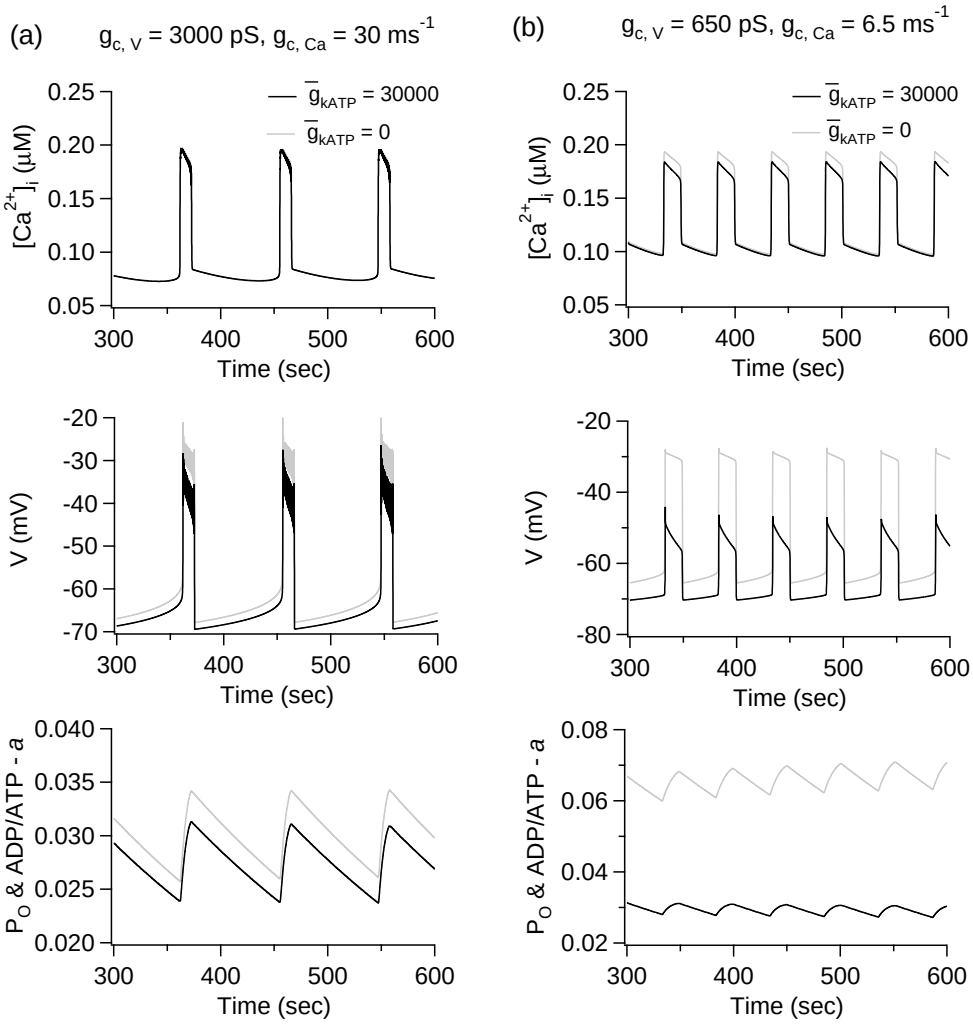
(a)
$g_{c,V}$ = 3000 pS, $g_{c,Ca}$ = 30 ms^{-1}
(b)
$g_{c,V}$ = 650 pS, $g_{c,Ca}$ = 6.5 ms^{-1}
$\bar{g}_{kATP}$ = 30000
$\bar{g}_{kATP}$ = 0
$[Ca^{2+}]_i$ (μM)
V (mV)
P_O & ADP/ATP - *a*
Time (sec)

Figure 5: